(Received 20 March 2026, Accepted 19 April 2026, Scheduled 2 May 2026)

A Compact Ultra-Wideband MIMO Antenna with Triple Band-Notched Characteristics

Zixiang Wang[1], Zhonggen Wang[1], Wenyan Nie[2,*], and Han Lin[1]

[1] *School of Electrical and Information Engineering, Anhui University of Science and Technology, Huainan 232001, China*
[2] *School of Mechanical and Electrical Engineering, Huainan Normal University, Huainan 232001, China*

ABSTRACT: This paper presents a compact four-port ultra-wideband (UWB) MIMO antenna with triple-band-notched characteristics. By introducing two types of resonators with distinct structures on both sides of the feed lines of the radiating elements, the proposed antenna achieves triple-band-notched functionality, thereby suppressing potential interference from WiMAX, C-band, and X-band. Notably, the spiral-shaped resonator simultaneously generates notch bands for both WiMAX and X-band, enabling a single structure to achieve multi-band-notched functionality and thereby enhancing the compactness and notch efficiency of the antenna design. Good agreement is observed between the simulated and measured results, validating the effectiveness and reliability of the proposed design. Across the entire operating band from 2.57 to 11.81 GHz (excluding the notch bands), the antenna exhibits a return loss below 10 dB, inter-port isolation greater than 20 dB, an envelope correlation coefficient (ECC) of less than 0.0095, and a diversity gain (DG) exceeding 9.9995 dB, fully satisfying the requirements of high-performance MIMO systems in terms of channel independence and transmission efficiency. The synergistic integration of multi-notch characteristics and high-performance metrics provides a novel technical approach for UWB-MIMO system design in complex electromagnetic environments.

1. INTRODUCTION

Ultra-wideband (UWB) technology, with its core features of high data rate transmission, high-precision positioning, and low-latency response, provides stable and reliable solutions for short-range wireless communication, positioning, tracking, and radar applications [1]. However, the extremely wide frequency spectrum of UWB systems inevitably overlaps with existing narrowband communication systems, such as Worldwide Interoperability for Microwave Access (WiMAX), Wireless Local Area Network (WLAN), and the X-band for satellite communications [3]. Interference signals from these bands can severely degrade the communication quality of UWB systems [4]. To mitigate such interference, designing antennas with band-notched characteristics has become a common practice. To date, various methods have been proposed to achieve notch characteristics, including closed-loop resonators, slots [5], stubs [6], stub-loaded resonators [7], and filter-embedded structures [8]. However, most existing UWB antenna designs employ notch structures that can only suppress a single interference band. For instance, the antenna in [9] achieves WLAN and X-band notches by etching two C-shaped slots on each radiator and a WiMAX notch by introducing an L-shaped slot on the ground plane. Nevertheless, multiple notch structures in a confined area may interfere with each other. Therefore, achieving multi-band notch functionality with a limited number of notch structures holds significant research importance [10]. Furthermore, while conventional UWB technology offers significant advantages in achieving high data rates and low cost, it inevitably suffers from the adverse effects of multipath propagation in practical applications [11]. The introduction of multiple-input multiple-output (MIMO) technology can effectively address this issue. However, MIMO antenna designs must tackle the mutual coupling problem among multiple antenna elements. To this end, researchers typically integrate various decoupling measures to enhance port isolation, thereby mitigating the impact of inter-element mutual coupling on system performance [12]. For example, diversity techniques, parasitic elements, defected ground structures (DGS) [13], electromagnetic bandgap structures, neutralization lines, and decoupling structures (DS) are all effective methods for improving isolation [14].

Addressing the aforementioned challenges in multi-band interference suppression and MIMO antenna design, this paper proposes a compact UWB MIMO antenna with triple-band-notched characteristics. By introducing a combination of spiral-shaped and C-shaped resonators adjacent to the feed lines, the proposed antenna successfully achieves precise band-notched suppression for three distinct frequency bands: WiMAX, C-band, and X-band. Notably, the spiral-shaped resonator simultaneously generates two notch bands, reducing the interaction between notch structures within a limited area. Both simulated and measured results demonstrate that the antenna maintains good port isolation and radiation performance while realizing triple-notch-band functionality, offering an efficient solution for UWB-MIMO communication systems operating in complex electromagnetic environments.

* Corresponding author: Wenyan Nie (wynie5240@163.com).

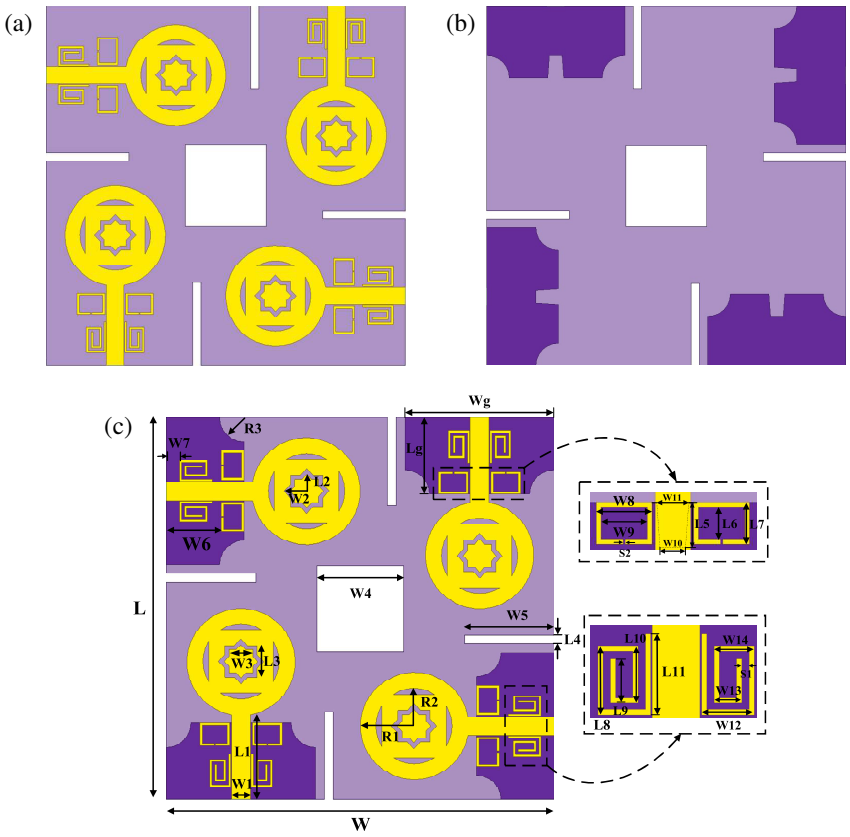

FIGURE 1. Geometry of the proposed UWB-MIMO antenna. (a) Top view; (b) Bottom view; (c) Detailed dimensional parameters.

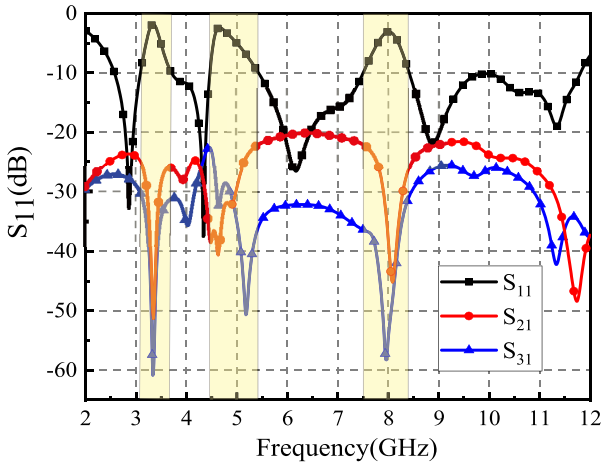

FIGURE 2. Simulated S-parameters of the proposed triple notched MIMO antenna characteristics.

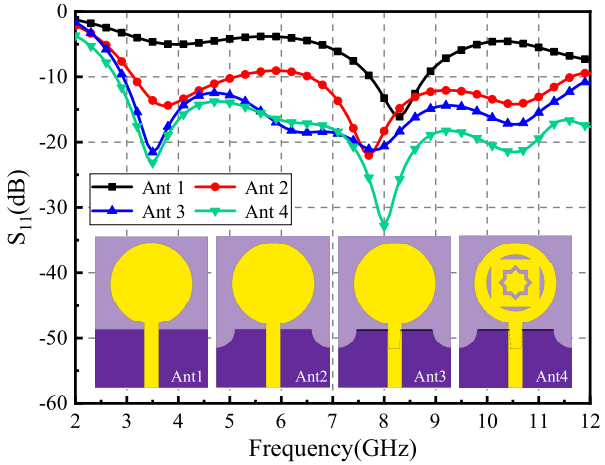

FIGURE 3. Design flow and S_{11} parameters of the monopole UWB antenna.

2. ANTENNA DESIGN PROCESS

2.1. Antenna Geometry

The geometry of the proposed UWB antenna is illustrated in Figure 1. The antenna is fabricated on an FR4 substrate with a relative permittivity of 4.4, a loss tangent of 0.02, and overall dimensions of 65 mm×65 mm×1.6 mm. As shown in Figure 1(a), the top layer of the substrate consists of four orthogonally arranged modified circular radiating elements. Spiral-shaped and C-shaped resonators are placed on both sides of the feed lines to generate the desired band-notched characteristics. As shown in Figure 1(b), the bottom layer comprises a rectangular ground plane, in which a DGS is employed to optimize the impedance matching across the operating band. Additionally, selective notching of the dielectric substrate is employed to enhance inter-port isolation. Detailed dimensional parameters of the proposed antenna, including critical geometric features of the etched slots, are annotated in Figure 1(c).

The final optimized dimensions are summarized in Table 1. Figure 2 illustrates the simulated S-parameters of the pro-

TABLE 1. Antenna parameter dimensions.

Parameter	W	W_1	W_2	W_3	W_4	W_5	W_6	W_7	W_8
Size (mm)	64	3.18	3.8	5.6466	14.6	15	9.2	2.2	5
Parameter	W_9	W_{10}	W_{11}	W_{12}	W_{13}	W_{14}	Wg	L	L_1
Size (mm)	4.2	2.3	2.9	3.18	1.5	2.34	25	64	14.5
Parameter	L_2	L_3	L_4	L_5	L_6	L_7	L_8	L_9	L_{10}
Size (mm)	2.8178	5.4	1.5	4.1	3	3.8	4.66	4.66	3.82
Parameter	L_{11}	L_{12}	Lg	R_1	R_2	R_3	S_1	S_2	
Size (mm)	5.5	5.5	13	9.1	6.4	4.1	0.84	0.2	

posed antenna. The simulation results demonstrate that the antenna achieves a well-matched impedance across the 2.57–11.81 GHz band. Furthermore, it successfully exhibits distinct band-notched characteristics at three targeted frequency bands: 3.09–3.70 GHz, 4.46–5.43 GHz, and 7.50–8.41 GHz. Throughout its entire operational bandwidth, the antenna maintains superior isolation performance, with inter-port isolation $|S_{ij}|$ exceeding 20 dB.

2.2. Proposed Single Antenna Evolution

The antenna design evolution is illustrated in Figure 3, along with the corresponding S_{11} curves at each design stage. To clearly describe the antenna evolution process, the stage antennas are designated as Antenna 1 through Antenna 4. The initial design, Antenna 1, consists of a circular radiating element with a radius of 9.1 mm and a rectangular ground plane. Simulation results show that it operates only from 7.72 to 8.81 GHz, indicating severe impedance mismatch outside this band. To improve the impedance matching characteristics across the entire frequency band, two symmetrical quarter-circular slots are etched into the ground plane of Antenna 2, forming a DGS. This modification guides and optimizes the current distribution on the ground plane, thereby significantly enhancing the impedance matching performance across the wide frequency band. Simulation results show that the operating band of Antenna 2 extends to 3.17–5.15 GHz and 6.6–11.64 GHz; however, its reflection coefficient does not yet fully cover the entire UWB band. The ground plane is further modified to alter current paths, yielding Antenna 3, which achieves 2.93–12 GHz coverage, fully covering the UWB band. To further broaden the bandwidth, the circular radiating element is truncated, resulting in Antenna 4. The final operating band extends from 2.77 GHz to 12 GHz, satisfying UWB and partial X-band requirements. This optimized antenna serves as the baseline for subsequent integration of notch-band structures.

2.3. Proposed Four-Port MIMO Antenna Evolution

To further enhance antenna reliability, signal quality, and data transmission rate, this section discusses the evolution of the four-port MIMO antenna. The monopole UWB antenna proposed in Section 2 is orthogonally arranged to form the initial four-port design, denoted as MIMO 1, with its structure shown in Figure 4(a). The antenna has overall dimensions of 65 mm×65 mm×1.6 mm, operates from 2.7 GHz to 12 GHz, and achieves inter-port isolation exceeding 17.4 dB. To further improve isolation, a defective substrate structure (DSS) is introduced based on MIMO 1, resulting in an enhanced design denoted as MIMO 2, as illustrated in Figure 4(b). The DSS modifies the electromagnetic field distribution around the antenna, particularly weakening the near-field coupling path, thereby effectively reducing mutual coupling through the dielectric substrate. The simulation results show that the port isolation of MIMO 2 is improved to over 21.5 dB.

Figures 5(a)–5(d) compare the electric field distributions with and without the DSS at 6.1 and 8.5 GHz, respectively. It can be clearly observed that without the DSS, a strong electric field is induced across the dielectric substrate. In contrast, when the DSS is present, these induced electric fields are effectively suppressed. This behavior occurs because the dielectric substrate acts as the primary propagation medium for surface waves. By etching slots in the substrate between adjacent antenna elements, obstacles are introduced directly into the surface wave propagation path. As a result, the transmission loss of surface waves is increased, and mutual coupling between antenna elements is effectively reduced. In summary, the proposed DSS design successfully enhances inter-port isolation, thereby contributing to a significant improvement in the overall performance of the MIMO system.

2.4. Notch Structure Design

To suppress narrowband interference within the UWB frequency range, a multi-band-notch structure is designed in this section. Owing to the high current density and significant current variations along the feed line, two types of resonators with distinct structures are introduced around the microstrip feed line to achieve triple-band-notched characteristics. The detailed design steps are illustrated in Figures 6(a) and 6(b), while Figure 6(c) presents the S_{11} parameters of the corresponding evolution.

First, a pair of symmetrical spiral resonators is placed on both sides beneath the feed line, as shown in Figure 6(a). These resonators absorb energy from the feed line through near-field coupling and generate a secondary radiation field out of phase with the primary radiation, resulting in destructive interference. Consequently, two notched bands are produced at 3.09–3.70 GHz (centered at 3.3 GHz) and 7.50–8.41 GHz (centered at 8.0 GHz), respectively. Subsequently, two identical C-shaped resonators are symmetrically positioned on both sides above the

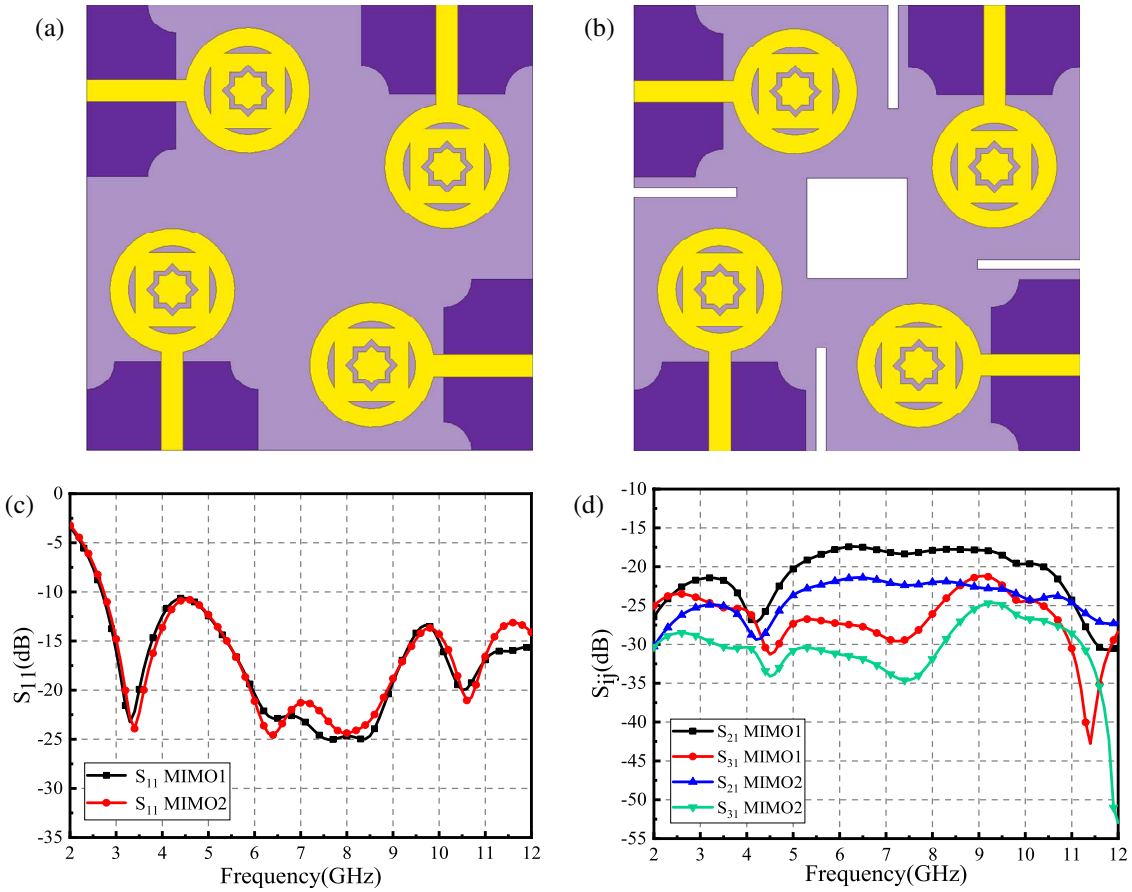

FIGURE 4. Effect of DSS on antenna S-parameters; (a) Without DSS; (b) With DSS; (c) S_{11} parameters of the antenna; (d) Isolation parameters of the antenna.

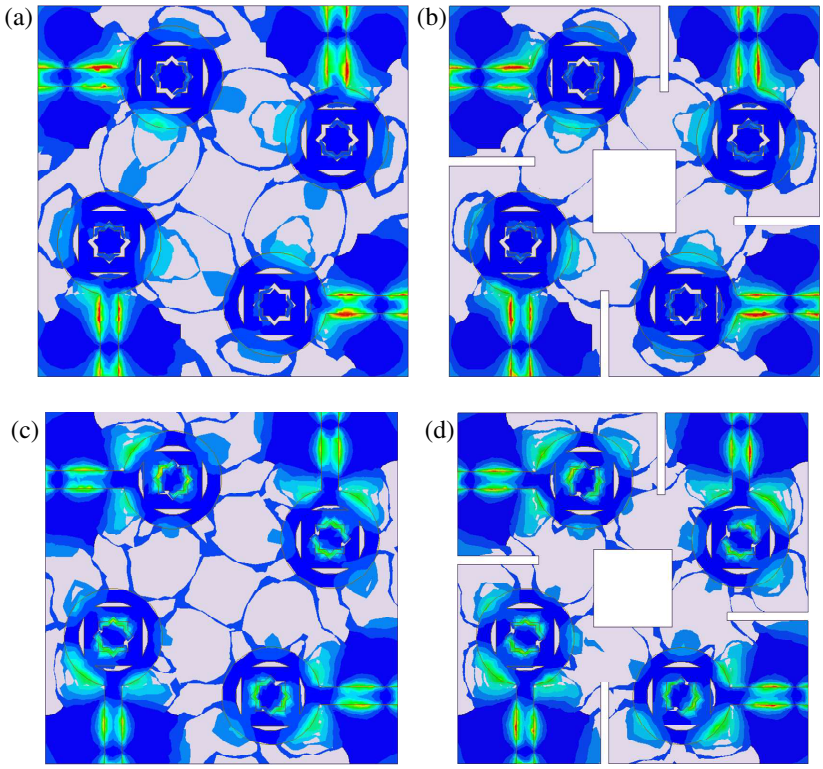

FIGURE 5. Antenna electric field diagrams; (a)–(b) without/with DSS at 6.1 GHz; (c)–(d) without/with DSS at 8.5 GHz.

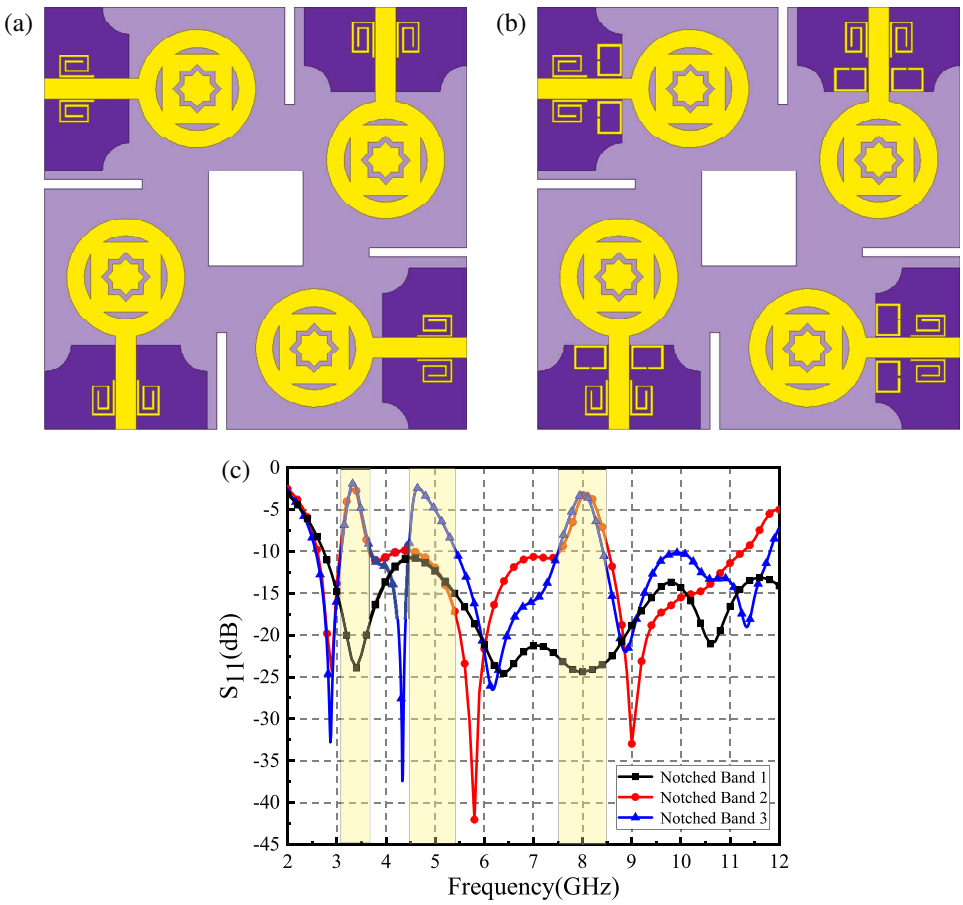

FIGURE 6. (a) Notched bands 1; (b) Notched bands 2; (c) S_{11} parameters.

feed line, as shown in Figure 6(b). These resonators concentrate the current at the corresponding frequencies around themselves, preventing the antenna from radiating energy within those bands. A third notch band is thus achieved at 4.46–5.43 GHz (centered at 4.6 GHz). The notch frequency of the C-shaped resonator can be approximately determined by the following half-wavelength resonance condition:

$$f_{notch} \approx \frac{c}{2L_{eff}\sqrt{\varepsilon_{eff}}} \tag{1}$$

where L_{eff} is the total length of the C-shaped resonator; c is the speed of light in vacuum; f_{notch} is the center frequency of the notch; and ε_{eff} is the dielectric constant of the substrate. Thus, the proposed antenna successfully realizes triple-band-notched characteristics, effectively suppressing interference from narrowband communication systems such as WLAN, while maintaining ultra-wideband operation from 2.57 to 11.81 GHz.

Figure 7 investigates the influence of different geometrical parameters of the proposed antenna on its notch-band characteristics. From Figure 7(a), it can be observed that as the parameter S_1 gradually decreases, the corresponding two notch bands shift from relatively higher frequencies to lower frequencies, while the notch bandwidth remains essentially unchanged. Similarly, as shown in Figure 7(b), by varying the value of S_2, the corresponding notch band also exhibits a shift from higher to lower frequencies. With the proposed design method, the positions of the notch bands can be effectively controlled simply by adjusting the geometric lengths of the resonators, thereby meeting various practical requirements. Furthermore, varying the parameters of the notch elements only affects the intended notch bands, with almost no impact on the return loss within the remaining UWB operating band, demonstrating the favorable independent tunability of the proposed notch structure.

2.5. Antenna Current Analysis

Surface current distribution reveals the operating state of each structural component at specific frequencies. At the notch center frequencies, current concentrates around the corresponding resonators while weakening in the main radiating element region, validating the notch characteristics. Figures 8(a)–8(c) show the simulated current distributions at 3.3 GHz, 4.6 GHz, and 8.0 GHz. At 3.3 GHz, current concentrates on the spiral resonator, suppressing radiation and forming a notch. At 4.6 GHz, current concentrates on the C-shaped resonator, preventing current from reaching the radiating element and creating a notch. At 8.0 GHz, current again concentrates on the spiral resonator, obstructing radiation and further confirming the notch. These results indicate that all three targeted bands excite effective resonances in their corresponding notch structures, achieving sig-

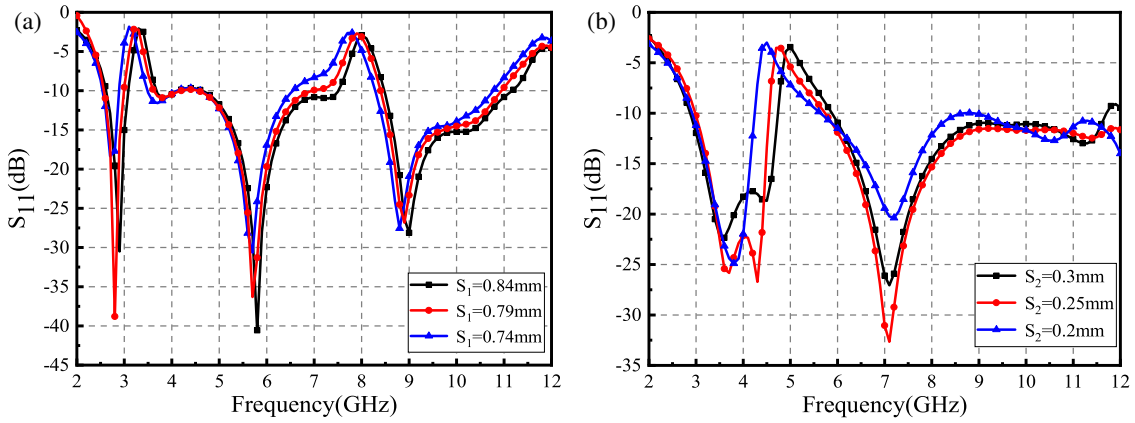

FIGURE 7. S-parameters for dimension variations; (a) S_1; (b) S_2.

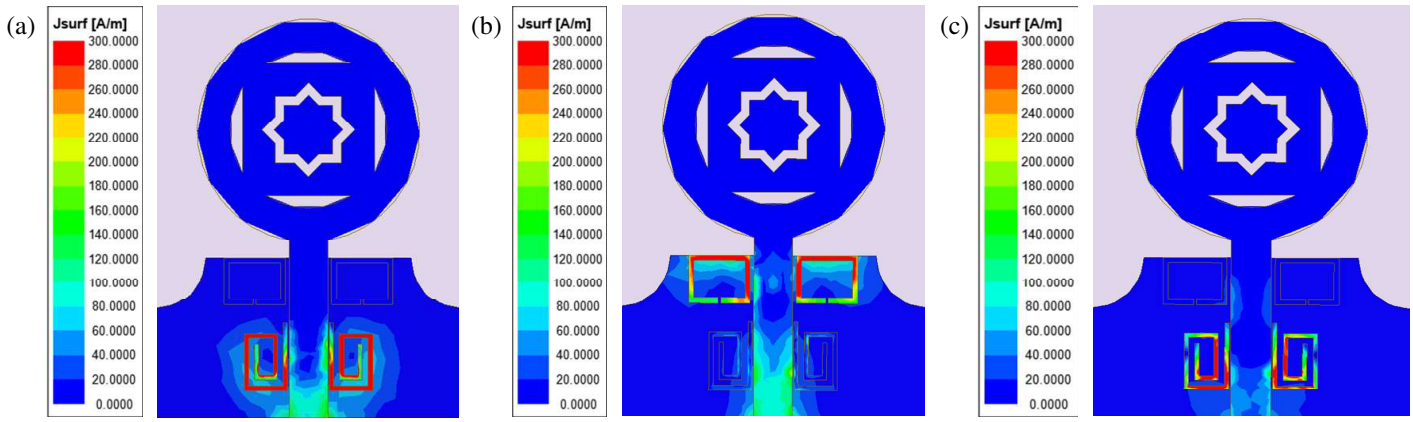

FIGURE 8. Current distribution diagram (a) 3.3 GHz; (b) 4.6 GHz; (c) 8.0 GHz.

nificant radiation suppression and fully verifying the functional effectiveness of the designed notch structures.

3. ANTENNA PERFORMANCE ANALYSIS

3.1. S-Parameter Analysis of the Antenna

The fabricated prototype is shown in Figure 9, and its S-parameters were measured using a vector network analyzer (VNA). As shown in Figure 10(a), the measured S_{11} agrees well with the simulated results, remaining below 10 dB across the 2.57–11.81 GHz band, except for the three notch bands (3.09–3.70 GHz, 4.46–5.43 GHz, and 7.50–8.41 GHz). The slight discrepancies are mainly due to SMA connector losses and fabrication tolerances. Figure 10(b) presents the isolation performance, where the S-parameters (S_{ij}) indicate that inter-port isolation exceeds 20 dB across the desired bandwidth, confirming the good port isolation of the proposed antenna.

3.2. Envelope Correlation Coefficient and Diversity Gain

Envelope correlation coefficient (ECC) is a key metric for evaluating channel correlation in MIMO antennas. A lower ECC indicates weaker antenna correlation. As ECC approaches zero, channels become nearly uncorrelated, with signals exhibiting independent fading envelopes. This ideal condition enhances system capacity, transmission reliability, and reduces interference and bit error rate. ECC can be calculated from S-parameters using the following formula:

$$\mathrm{ECC} = \frac{\left|S_{ii} * S_{ij} + S_{ji} * S_{jj}\right|^2}{\left(1 - |S_{ii}|^2 - S_{ij}^2\right)\left(1 - |S_{ji}|^2 - S_{jj}^2\right)} \tag{2}$$

Diversity gain (DG) characterizes the diversity order of spatial channels, enabling a more stable signal-to-noise ratio (SNR) and more reliable reception. Multipath effects are a prerequisite for DG; without them, DG cannot provide its unique advantages. Thus, DG not only demonstrates improved signal stability but also reflects the ability of MIMO systems to mitigate multipath effects. DG can be calculated from ECC using the following equation:

$$\mathrm{DG} = 10\sqrt{1 - \mathrm{ECC}^2} \tag{3}$$

As shown in Figure 11, the ECC stays below 0.0095, and the DG exceeds 9.9995 dB across the operating band, fully meeting the design requirements. These results confirm that the proposed antenna elements have very low correlation and excellent diversity performance, ensuring non-interfering operation and higher transmission efficiency.

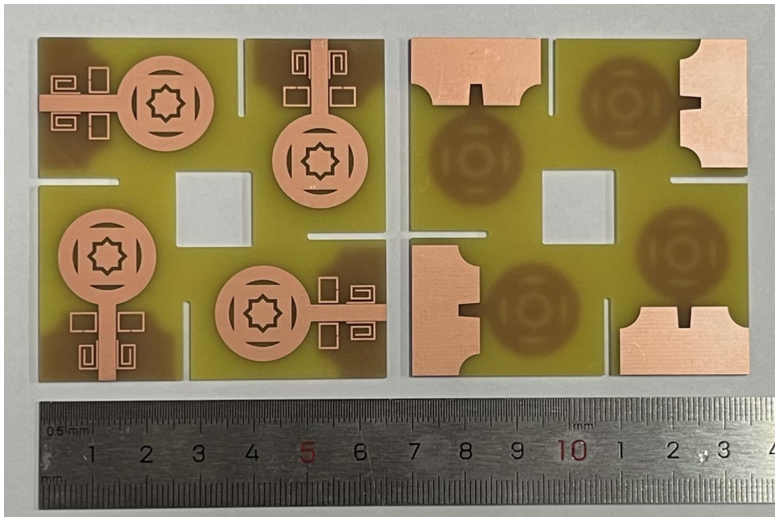

FIGURE 9. The fabricated prototype of the proposed antenna .

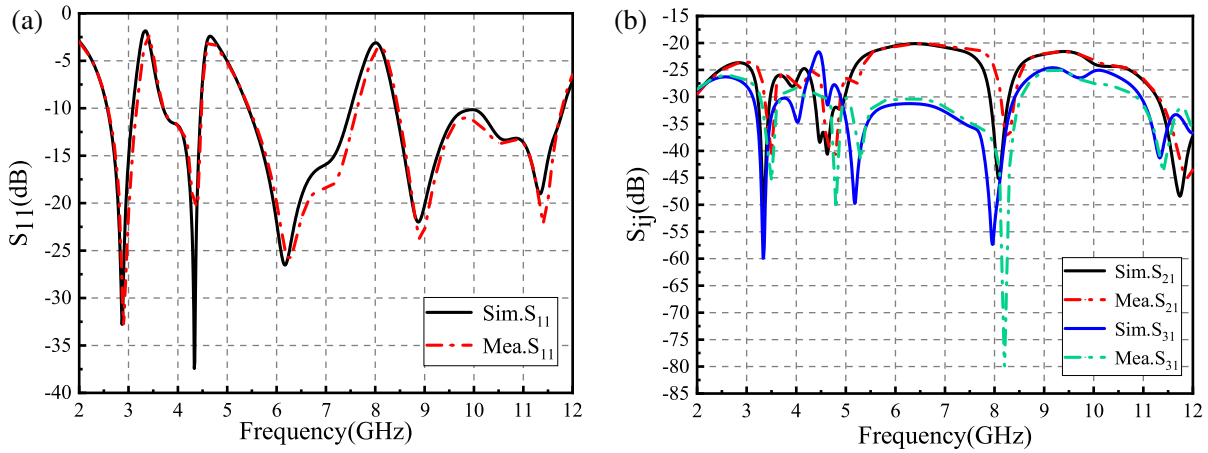

FIGURE 10. Simulated and measured S-parameters of the proposed antenna: (a) S_{11}, (b) S_{21} and S_{31}.

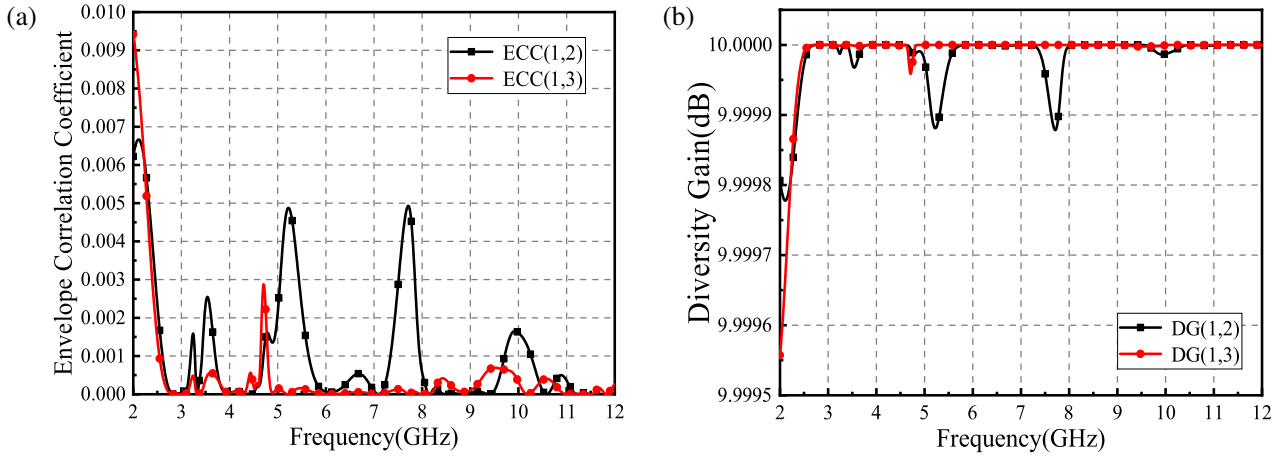

FIGURE 11. (a) ECC; (b) DG.

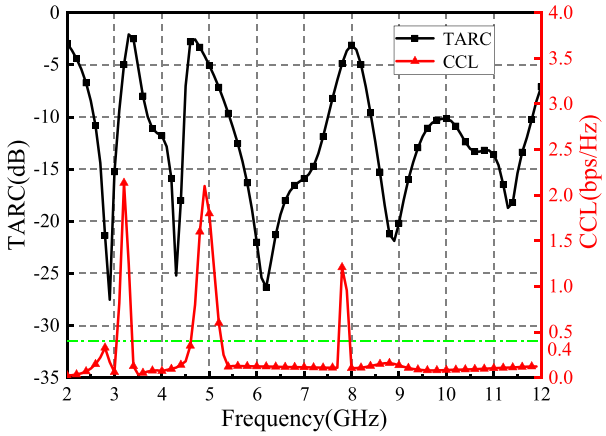

FIGURE 12. TARC and CCL.

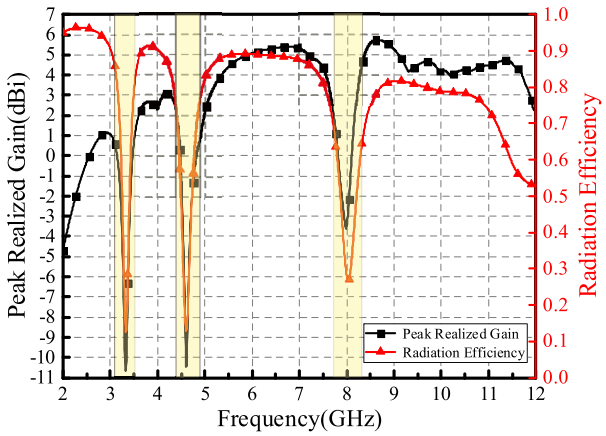

FIGURE 13. Antenna peak realized gain and radiation efficiency.

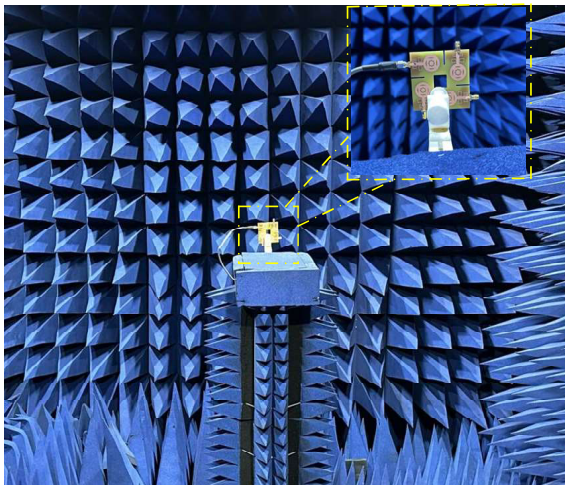

FIGURE 14. Measured results in microwave anechoic chamber.

3.3. Total Active Reflection Coefficient and Channel Capacity Loss

For MIMO antenna systems, S-parameters alone cannot fully predict real-world performance. Therefore, the total active reflection coefficient (TARC) is necessary. TARC can be calculated from S-parameters using the following formula:

$$\text{TARC} = \frac{\sqrt{\sum_{i=1}^{4}\left|S_{i1} + \sum_{n=2}^{4} S_{in}e^{j\theta_{n-1}}\right|^2}}{2} \tag{4}$$

Channel capacity loss (CCL) is also a critical parameter for MIMO antennas. Generally, a CCL value of less than 0.4 bps/Hz meets the design requirements of MIMO antennas. CCL is expressed as:

$$\text{CCL} = -\log_2 \det\left|\psi^R\right| \tag{5}$$

$$\psi^R = \begin{pmatrix} \rho_{11} & \cdots & \rho_{1n} \\ \vdots & \ddots & \vdots \\ \rho_{m1} & \cdots & \rho_{mn} \end{pmatrix} \tag{6}$$

The calculated results, shown in Figure 12, clearly indicate that for the proposed UWB-MIMO antenna, except within the notch bands, the TARC remains below 10 dB, and the CCL stays below 0.4 bps/Hz. This further demonstrates the antenna's very low coupling, effectively ensuring channel independence without mutual interference during signal transmission and reception, thereby significantly enhancing overall system capacity.

3.4. Radiation Performance Analysis of the Antenna

Figure 13 presents the peak realized gain and radiation efficiency of the four-port MIMO antenna. Across the operating band (excluding notch bands), the gain ranges from 1 to 5.8 dBi, and the radiation efficiency remains high. At the three notch center frequencies (3.3 GHz, 4.6 GHz, and 8.0 GHz), the gain drops sharply to -10.6 dBi, -10.4 dBi, and -3.7 dBi, with corresponding efficiencies of 12%, 13%, and 26%, directly confirming successful band-notched functionality. As explained by the surface current distribution in Figure 8, at non-notch frequencies, current concentrates on the main radiating elements. At notch frequencies, current becomes strongly localized around the corresponding resonators. These resonators

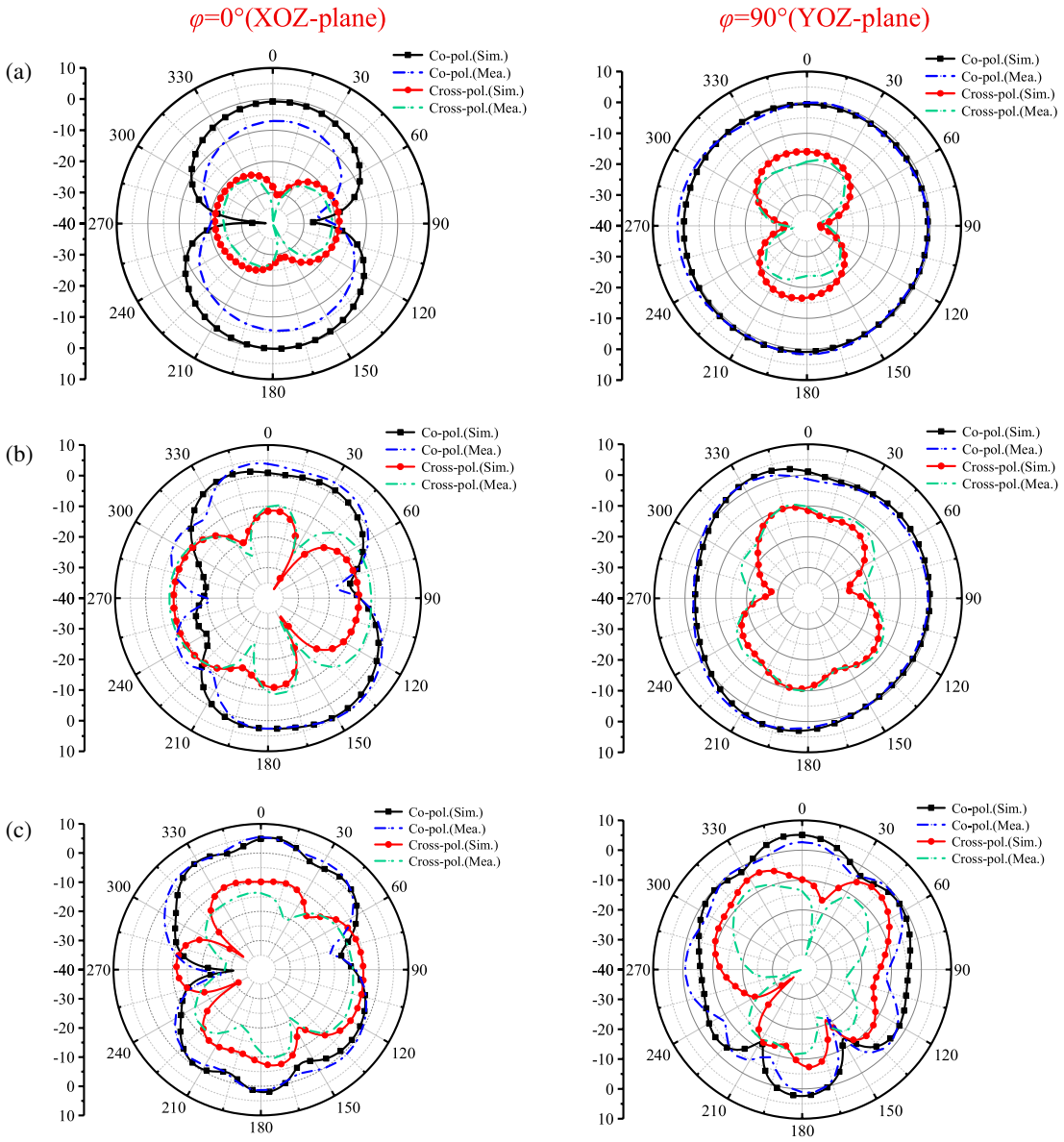

FIGURE 15. Simulation and measurement radiation patterns. (a) 4.3 GHz; (b) 6.1 GHz; (c) 8.8 GHz.

TABLE 2. Comparison of the proposed antenna with several existing antennas.

Ref.	Size	BW(GHz)	No. of notches	No. of Ports	Isolation (dB)	ECC	A structure generates multiple notches
[15]	$0.91\lambda_0 \times 0.91\lambda_0$	3.4–8.25	0	4	< -25	<0.01	NO
[16]	$0.44\lambda_0 \times 0.48\lambda_0$	3.0–12.0	3	4	< -20	<0.16	NO
[17]	$0.53\lambda_0 \times 0.53\lambda_0$	2.03–15.04	3	4	< -20	<0.05	NO
[18]	$0.56\lambda_0 \times 0.56\lambda_0$	2.1–20	2	4	< -25	<0.02	NO
[19]	$0.75\lambda_0 \times 0.75\lambda_0$	3.2–11.2	0	4	< -20	<0.004	NO
[20]	$0.60\lambda_0 \times 0.60\lambda_0$	3.0–11.0	2	4	< -17	<0.03	NO
This	$\mathbf{0.56\lambda_0 \times 0.56\lambda_0}$	**2.57–11.81**	**3**	**4**	$\mathbf{< -20}$	**< 0.0095**	**YES**

Where $\lambda\times$ is the free-space wavelength at the lowest operating frequency.

capture electromagnetic energy through near-field coupling and generate out-of-phase secondary radiation, thereby confining the energy around themselves and preventing it from radiating into free space. Outside the notch bands, stable gain and high

efficiency are maintained, confirming that the notch structures do not degrade overall performance.

The radiation patterns were measured in a fully anechoic chamber using a standard-gain horn antenna as the reference, with the complete measurement setup shown in Figure 14.

Figure 15 presents the two-dimensional radiation patterns of the proposed four-port ultra-wideband antenna at 4.3 GHz, 6.1 GHz, and 8.8 GHz. The results show that at the lower frequency of 4.3 GHz, the antenna exhibits good omnidirectional radiation in the YOZ-plane and a typical bidirectional radiation pattern in the XOZ-plane. As the frequency increases, influenced by the increased electrical size of the antenna and the excitation of higher-order modes, the radiation patterns exhibit slight distortion and ripples; nevertheless, they maintain stable and effective radiation coverage overall. In terms of polarization purity, the cross-polarization level is significantly lower than the co-polarization level in the main radiation directions, with a difference of 15–20 dB, indicating that the antenna possesses good polarization isolation and meets the requirements for multi-port system operation. Furthermore, at all measured frequencies, the simulated and measured co-polarization and cross-polarization radiation patterns are in good agreement. This consistency fully validates the design rationality and practical radiation performance of the proposed antenna.

A comprehensive comparison between the proposed antenna and various advanced reported designs is conducted, with the key performance metrics summarized in Table 2. An in-depth analysis reveals that, within a compact footprint, the proposed antenna not only achieves excellent ECC and maintains port isolation below 20 dB but also realizes triple-band-notched characteristics with fewer notch structures. Specifically, a single spiral-shaped resonator simultaneously generates two notch bands (centered at 3.3 GHz and 8.0 GHz) — an advantage not possessed by most existing designs. This fully demonstrates that the proposed design strikes an excellent balance among multi-band interference suppression, MIMO performance, and structural simplicity, offering a certain reference value among similar antenna designs.

4. CONCLUSION

This study proposes and validates a compact four-port UWB MIMO antenna with triple-band-notched characteristics. By combining spiral and C-shaped resonators adjacent to the feed lines, the antenna precisely suppresses narrowband interference from WiMAX, C-band, and X-band. Within the notch bands, the radiation efficiency drops to 12%, 13%, and 26%, respectively, demonstrating effective suppression. While maintaining the UWB operating band (2.57–11.81 GHz), the antenna achieves excellent MIMO performance with an ECC below 0.0095 and DG exceeding 9.9995 dB. Good agreement between simulated and measured results validates the design's feasibility and effectiveness. In conclusion, the proposed antenna successfully realizes the synergistic design of wideband coverage, multi-band notch characteristics, and excellent MIMO performance, positioning it as an ideal candidate for future wireless communication systems.

ACKNOWLEDGEMENT

This work was supported in part by the Natural Science Research Project of Anhui Educational Committee under Grant No. 2025AHGXZK31006, in part by the Research Foundation of Jiangsu Engineering Research Center for Bionics Control Technology and Equipment under No. FSKZ202503, in part by the Anhui International Joint Research Center for Ancient Architecture Intellisencing and Multi-Dimensional Modeling under No. GJZZX2025KF03.

REFERENCES

[1] Vendik, I. B., A. Rusakov, K. Kanjanasit, J. Hong, and D. Filonov, "Ultrawideband (UWB) planar antenna with single-, dual-, and triple-band notched characteristic based on electric ring resonator," *IEEE Antennas and Wireless Propagation Letters*, Vol. 16, 1597–1600, 2017.

[2] Tu, R., H. Lin, and Z. Wang, "A mimo ultra-wideband antenna with high isolation and triple notches," *Progress In Electromagnetics Research C*, Vol. 159, 91–102, 2025.

[3] Li, W.-A., Z.-H. Tu, Q.-X. Chu, and X.-H. Wu, "Differential stepped-slot UWB antenna with common-mode suppression and dual sharp-selectivity notched bands," *IEEE Antennas and Wireless Propagation Letters*, Vol. 15, 1120–1123, 2016.

[4] Salamin, M. A., S. Das, and A. Zugari, "Closed loop resonator based compact UWB antenna with single notched band varying between WLAN and X-band for UWB applications," *Frequenz*, Vol. 74, No. 5-6, 201–209, 2020.

[5] Jairath, K., N. Singh, V. Jagota, and M. Shabaz, "Compact ultrawide band metamaterial-inspired split ring resonator structure loaded band notched antenna," *Mathematical Problems in Engineering*, Vol. 2021, No. 1, 5174455, May 2021.

[6] Doddipalli, S. and A. Kothari, "Compact UWB antenna with integrated triple notch bands for WBAN applications," *IEEE Access*, Vol. 7, 183–190, 2019.

[7] Iqbal, A., A. Smida, N. K. Mallat, M. T. Islam, and S. Kim, "A compact UWB antenna with independently controllable notch bands," *Sensors*, Vol. 19, No. 6, 1411, 2019.

[8] Liu, L., S. W. Cheung, and T. I. Yuk, "Compact MIMO antenna for portable UWB applications with band-notched characteristic," *IEEE Transactions on Antennas and Propagation*, Vol. 63, No. 5, 1917–1924, 2015.

[9] Jayant, S. and G. Srivastava, "Close-packed quad-element triple-band-notched UWB MIMO antenna with upgrading capability," *IEEE Transactions on Antennas and Propagation*, Vol. 71, No. 1, 353–360, 2023.

[10] Zhao, Z., C. Zhang, Z. Lu, H. Chu, S. Chen, M. Liu, and G. Li, "A miniaturized wearable antenna with five band-notched characteristics for medical applications," *IEEE Antennas and Wireless Propagation Letters*, Vol. 22, No. 6, 1246–1250, 2023.

[11] Ren, J., W. Hu, Y. Yin, and R. Fan, "Compact printed MIMO antenna for UWB applications," *IEEE Antennas and Wireless Propagation Letters*, Vol. 13, 1517–1520, 2014.

[12] Sharbati, V., X. Bao, J. J. Healy, N. Zhang, K. Nadali, and M. J. Ammann, "Dynamic tuning of notch bands in UWB antenna based on liquid metal for cognitive radio applications," *IEEE Antennas and Wireless Propagation Letters*, Vol. 23, No. 12, 4708–4712, 2024.

[13] Zhao, L., Y. Wang, C. Liu, D. Song, C. Hu, C. Li, H. Zhao, and Z. Wang, "Compact circular-shaped MIMO antenna covers UWB bandwidth with four frequently-used band-notched characteristics for multi-scenario applications," *IEEE Access*,

Vol. 12, 32 762–32 771, 2024.

[14] Chen, Z., W. Zhou, and J. Hong, "A miniaturized MIMO antenna with triple band-notched characteristics for UWB applications," *IEEE Access*, Vol. 9, 63 646–63 655, 2021.

[15] Ghosh, A., A. Ghosh, and J. Kumar, "Circularly polarized wideband quad-element MIMO antenna with improved axial ratio bandwidth and mutual coupling," *IEEE Antennas and Wireless Propagation Letters*, Vol. 23, No. 12, 4718–4722, 2024.

[16] Sushma, T., R. Gogineni, N. V. Ratnam, S. R. Babu, S. Mandava, and P. V. K. Kanth, "A miniaturized quad port highly isolated triple band notched UWB-MIMO diversity antenna," *Progress In Electromagnetics Research C*, Vol. 152, 43–53, 2025.

[17] El-Gendy, M. S., M. M. M. Ali, E. B. Thompson, and I. Ashraf, "Triple-band notched ultra-wideband microstrip MIMO antenna with bluetooth band," *Sensors*, Vol. 23, No. 9, 4475, 2023.

[18] Rekha, V. S. D., P. Pardhasaradhi, B. T. P. Madhav, and Y. U. Devi, "Dual band notched orthogonal 4-element MIMO antenna with isolation for UWB applications," *IEEE Access*, Vol. 8, 145 871–145 880, 2020.

[19] Yao, Y., Y. Shao, J. Zhang, and J. Zhang, "A transparent antenna using metal mesh for UWB MIMO applications," *IEEE Transactions on Antennas and Propagation*, Vol. 71, No. 5, 3836–3844, 2023.

[20] He, L., Y. Miao, and G. Liu, "A compact 4×4 UWB MIMO antenna with 5G and WLAN band rejected operation," *Progress In Electromagnetics Research C*, Vol. 156, 39–47, 2025.